Detailed Atomistic Molecular Dynamics Simulation of *cis*-1,4-Poly(butadiene)

Georgia Tsolou,[†,§] Vlasis G. Mavrantzas,[*,†,‡,§] and Doros N. Theodorou[†,∥]

Institute of Chemical Engineering and High-Temperature Chemical Processes (FORTH-ICE/HT), Patras GR 26504, Greece, Department of Chemical Engineering, University of Patras, Patras GR 26504, Greece, Interdepartmental EPEAEK Program on Polymer Science and Technology, University of Patras, Patras GR 26504, Greece, and Department of Materials Science and Engineering, School of Chemical Engineering, National Technical University of Athens, 157 80 Athens, Greece

Received May 5, 2004; Revised Manuscript Received November 15, 2004

ABSTRACT: Well-relaxed atomistic configurations of model *cis*-1,4-poly(butadiene) (PB) systems, ranging in molecular length from C_{32} to C_{400}, have been subjected to detailed molecular dynamics simulations in the NPT ensemble for times up to 600 ns. Results are presented for the static and (mainly) dynamic properties of these systems, such as the segmental and terminal relaxation properties, the self-diffusion coefficient, D, and the single-chain dynamic structure factor, $S(q,t)$, at pressure $P = 1$ atm and temperatures, T, between 298 and 430 K. Our simulation data demonstrate that, around C_{200}, D is seen to exhibit a change in its power-law dependence on molecular weight, M, deviating from a Rouse (where $D \approx M^{-b}$ with $b \cong 1$) toward a reptation-like (where $D \approx M^{-b}$ with $b \cong 2.1$) behavior. Following the methodology introduced by Harmandaris et al. [*Macromolecules* **2003**, *36*, 1376] for linear polyethylene (PE) melts, we have further been able to successfully project atomistic *cis*-1,4-PB chain configurations to primitive paths, thereby mapping simulation trajectories onto the reptation model. This has allowed us to consistently calculate the friction coefficient, ζ, per carbon atom of *cis*-1,4-PB melts both below and above the molecular weight for the formation of entanglements. The dependence of D on T is also presented.

I. Introduction

Polydienes, such as poly(butadiene) (PB) and poly(isoprene) (PI), play a very important role in chemical technology. This has led to the accumulation of a wealth of available experimental data for their structural, conformational, and dynamic properties and their dependence on microstructure (1,4 versus 1,2) and configuration (cis versus trans). Motivated by the wide applications of PB and PI, in particular, in the automotive and electronics industries and in rubber technology, we have recently undertaken a systematic investigation of the structure−property relationships in these two polymers through detailed simulations at the atomistic level. These investigations complement a large body of experimental and simulation data for the two polymers, the latter dating back to 1966, when Mark published his first results on the random-coil configuration of *cis*-1,4-PB and *cis*-1,4-PI using the rotational isomeric state (RIS) model.[1] Mark's studies were extended by Abe and Flory[2] to include trans monomers. The structure (including the static free volume) properties of 1,4-PB melts were subsequently studied by Mattice and coworkers[3−5] with molecular mechanics and molecular dynamics techniques. These were followed by MD investigations of conformational dynamics and chain relaxation properties of bulk PB melts by Gee and Boyd[6] and Han et al.[7] The static and dynamic properties of *cis*-1,4-PB have also been studied by Okada and Furuya[8] through an MD simulation of a single 200 monomer chain system by employing a very detailed atomistic model that accounts also for electrostatic interactions. Detailed results concerning the decay of all torsional autocorrelation functions at several temperatures were also calculated to quantify conformational transitions in the *cis*-1,4-PB chain.

The more-recent MD work of Smith and Paul[9] and Smith et al.[10−13] has included simulations with a new united-atom force field based on quantum chemistry calculations[9] that allowed a thorough study of both the local[10] and global dynamics[11−13] of 1,4-PB melts. The atomistic MD simulation results were compared to ^{13}C NMR and neutron spin−echo (NSE) measurements and used for the evaluation of the predictions of the Rouse model[14,15] and other more-recent theories[16] accounting for chain stiffness. Describing the time autocorrelation functions of the normal modes with single exponentials was supported neither by the simulation results nor by the experimental measurements. The Rouse model was further seen to offer inaccurate descriptions of the simulation and experimental data for the dynamic structure factor, $S(q,t)$. The origin of this failure was attributed to the non-Gaussian displacements of the chain segments, which were considered to be responsible for the deviations from the Rouse behavior.[13]

In a more-recent study, Byutner and Smith[17] proposed a method for calculating the viscoelastic properties of high-molecular-weight PB melts using as input the results of atomistic simulations with smaller-molecular-weight systems.

From the point of view of experimental investigations (and restricting our literature survey to PB, on which the present simulation study will focus), attention has been paid to the development of techniques for the measurement of rheological properties, such as the plateau modulus, G_N^0, and the zero shear rate viscosity,

* Author to whom correspondence should be addressed. E-mail: vlasis@chemeng.upatras.gr. Tel: +30-2610-997-398. Fax: +30-2610-965-223.

† Institute of Chemical Engineering and High-Temperature Chemical Processes.

‡ Department of Chemical Engineering, University of Patras.

§ Interdepartmental EPEAEK Program on Polymer Science and Technology, University of Patras.

∥ National Technical University of Athens.

10.1021/ma0491210 CCC: $30.25
Published on Web 01/21/2005

η_0, and for the estimation of the critical molecular weights, M_e and M_c, marking the passage from the Rouse to the entangled regime.[18−23] Measurements have been performed with both polydisperse and monodisperse[18] 1,4-PB samples and with different microstructures[19,21] in an effort to understand the effect of the relative cis/trans content on polymer viscoelasticity. Roovers[22] measured the viscoelastic properties of linear, high-molecular-weight polybutadienes at different temperatures and documented the validity of the scaling laws characterizing the dependence of η_0 on M. He concluded that, for molecular weights well above M_c, $\eta_0 \approx M^{3.4}$, in agreement with the predictions of the modified reptation theory that incorporates contour length fluctuations.[24] Colby et al.[23] extended Roover's study to a wider range of molecular weights, including viscosity measurements of PB with several linear viscoelastic techniques, such as stress relaxation and capillary viscometry, at different temperatures.

In parallel to rheological measurements, techniques such as NMR[10,25−33] and neutron scattering[12,34−37] have been employed to probe local and global dynamics in high-molecular-weight PB systems. Proofs for the existence of topological constrains have been reported,[25] and the predictions of reptation theory have been evaluated.[26,31] Fleischer and Appel,[27] for example, measured the self-diffusion coefficient in PB and PI samples and confirmed the slowing-down of the self-diffusion process for molecular weights above M_e. A similar study was undertaken a few years later by Klein et al.[29] in an effort to evaluate the limits of validity of the Rouse and reptation theories for linear PB samples.

Very recently, Guillermo and Cohen Addad[32] carried out NMR measurements of the self-diffusion coefficient in both short and long PB chains which supported that the crossover from a Rouse-like to a reptation-like dynamics occurs at a molecular weight (almost 15 times the M_e value) much higher than that calculated from stress−relaxation experiments. In the longer-chain systems, a power law of the form $D \approx M^{-2.4\pm0.05}$ was observed to describe quite well the experimental data in agreement with previous experimental measurements[38] and MD simulation results with PE melts.[39] In a subsequent study,[33] the same researchers showed that, in a polymer chain, two qualitatively distinct random motions take place: the first concerns the motion of end-chain segments, which behave like short chains, and the second concerns the motion of inner segments, which is less isotropic. They also found that accepting an effective segmental friction coefficient which scales with the molecular weight as $M^{0.3}$ leads to the same power laws for the molecular-weight dependence of the zero-shear rate viscosity, η_0, and diffusion coefficient, D, as those predicted by the modified reptation theory.

From the quick literature survey, it appears that, despite the quite large number of simulation efforts, the longest *cis*-1,4-PB melt that has been simulated so far by a dynamic method under true bulk conditions is C_{114}.[11] The reason for this should be sought in the problem of long relaxation times that plagues dynamic studies and limits the accessible simulation time scales to times under 200 ns. It is the objective of this work to extend these limits to higher *cis*-1,4-PB systems and longer times through the implementation of an efficient simulation methodology that uses robust Monte Carlo (MC) algorithms to pre-equilibrate the system, execution of long MD simulation runs with a multiple time step algorithm, and calculation of the dynamic properties of the system either directly from the MD simulation or indirectly by mapping atomistic trajectories onto a suitable mesoscopic model.[40] Such a methodology has so far been applied to simulate the dynamic and some of the rheological properties of linear polyethylene (PE) melts of molecular weight up to 3500 g mol^{-1} with remarkable success;[39] it is extended here to *cis*-1,4-PB.

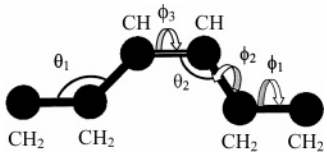

Figure 1. United-atom model of *cis*-1,4-PB. The bending angles are denoted as θ_1 and θ_2 and the dihedrals as ϕ_1, ϕ_2, and ϕ_3.

This paper is organized as follows. Section II discusses the molecular model used in the atomistic MD simulations and the systems simulated. Section III outlines the key points of the simulation methodology followed to track the dynamics of these systems for longer times. Results concerning the static and (mainly) the dynamic properties of *cis*-1,4-PB are presented in detail in Section IV. The paper concludes with Section V discussing the major findings of the present work and future plans.

II. Molecular Model Systems Studied

A united-atom description is used in this work to represent the *cis*-1,4-PB chains, according to which each carbon atom in a monomer together with all hydrogens attached to it is considered as a single Lennard−Jones interaction site (see Figure 1). Bond-stretching interactions are described by harmonic potential functions of the form

$$U_{\text{stretching}}(l) = \frac{k_{\text{str}}}{2}(l - l_0)^2 \tag{1}$$

with the values of the parameters k_{str} and l_0 describing the stiffness of the harmonic spring and the equilibrium bond length for the three different types of bonds in the *cis*-1,4-PB molecule borrowed from the work of Gee and Boyd, respectively;[6] they are summarized here in Table 1. Bond-bending potentials of the form

$$U_{\text{bending}}(\theta) = \frac{k_\theta}{2}(\theta - \theta_0)^2 \tag{2}$$

have also been used to describe the interactions associated with the two bending angles, θ_1 and θ_2 (see Figure 1), with k_θ and θ_0 values borrowed from the work of Smith and Paul;[9] these are the same as those used by Gee and Boyd[6] and are summarized here in Table 1. The torsional potentials associated with the three dihedral angles, ϕ_1, ϕ_2, and ϕ_3 (see Figure 1), have also been taken from the work of Smith and Paul[9] and are of the form

$$U_{\text{torsional}}(\phi) = \frac{1}{2}\sum_{n=1}^{6} k_n(1 - \cos(n\phi)) \tag{3}$$

with the three sets of the coefficients k_n reported in Table 1. Nonbonded interactions (intermolecular and intramolecular for all atom pairs separated by more

Table 1. Values of the Force Field Parameters Defining The (a) Stretching (Taken from Ref 6), (b) Bending (Taken from Ref 9), (c) Torsional (Taken from Ref 9), and (d) Lennard−Jones (Taken from Ref 9) Potential Functions

(a)

stretching	k_{str} (kcal (mol Å^2)$^{-1}$)	l_0 (Å)
CH_2-CH_2	663	1.54
CH_2-CH	769	1.50
CH=CH	1033	1.34

(b)

bending	k_θ (kcal mol^{-1})	θ_0 (deg)
CH_2-CH_2-CH	115	111.65
$CH_2-CH-CH$	89.4	125.89

(c)

torsion	k_1 (kcal mol^{-1})	k_2 (kcal mol^{-1})	k_3 (kcal mol^{-1})	k_4 (kcal mol^{-1})	k_5 (kcal mol^{-1})	k_6 (kcal mol^{-1})
$CH_2-CH=CH-CH_2$		24.2				
$CH_2-CH_2-CH=CH$	1.033	−0.472	0.554	0.263	0.346	0.164
$CH-CH_2-CH_2-CH$	−0.888	−0.619	−3.639	−0.066	−0.247	−0.190

(d)

nonbonded	ϵ (kcal mol^{-1})	r_{min} (Å)
CH_2-CH_2	0.0936	4.500
CH_2-CH	0.1000	3.800
CH=CH	0.1015	4.257

Table 2. System Parameters for the *cis*-1,4-PB Melts Simulated in This Work

N	N_{ch}	I	T (K)
32	168	1.08	298, 343, 353, 413
48	80	1.08	298, 343, 353, 413
56	56	1.05	413
64	64	1.08	298, 343, 353, 413
80	40	1.05	298, 343, 353, 413
96	40	1.08	298, 343, 353, 413, 430
112	32	1.05	343, 413, 430
128	32	1.08	413
140	32	1.05	298, 353, 413, 430
160	24	1.05	413
200	32	1.08	413
240	32	1.08	413
320	32	1.08	413
400	32	1.05	413

than three bonds) have been described by a Lennard−Jones potential of the form

$$U_{LJ}(r) = \epsilon\left[\left(\frac{r_{min}}{r}\right)^{12} - 2\left(\frac{r_{min}}{r}\right)^{6}\right] \quad (4)$$

with the values of the constants ϵ and r_{min} summarized in Table 1.[9]

With the force field described by eqs 1−4, a large number of model *cis*-1,4-PB systems were simulated whose characteristics (average chain length, N, total number of chains, N_{ch}, polydispersity index, I, and temperature, T, at which the simulation was carried out) are listed in Table 2. The distribution of chain lengths in all systems was selected to be uniform, with chain lengths varying between a lower and a higher value yielding the polydispersity indices reported in Table 2. For all systems, initial configurations were borrowed from end-bridging Monte Carlo (EBMC) simulations[41,42] of similar model systems.

The MD simulations were carried out in the isothermal−isobaric (NPT) statistical ensemble, with the numbers of all chain species present in the system fixed. To maintain the temperature, T, and pressure, P, fixed at their prescribed values, the Nosé−Hoover[43,44] thermostat−barostat was used. Most simulations were carried out at $P = 1$ atm and $T = 413$ K; however, as Table 2 shows, many of the systems were also simulated at other temperatures in the interval [298, 430 K]. For each set of chain-length distribution and temperature−pressure conditions, only one MD simulation was carried out, i.e., only one initial configuration produced by the EBMC simulation was subjected to MD. Such an initial configuration was carefully chosen so as to have practically a uniform chain-length distribution, a density equal to the mean melt density of the simulated system at the temperature and pressure conditions of the computational experiment, and a square end-to-end distance equal to the mean-square chain end-to-end distance, $\langle R^2 \rangle$, of the simulated cis-1,4-PB system.[41]

For the integration of the equations of motion, the multiple-time-step algorithm RESPA[45,46] was used. This algorithm separates the fast degrees of freedom (bond stretching, angle bending, torsional vibrations) from the slow degrees of freedom (nonbonded interactions). The fast degrees of freedom are integrated with a smaller time-step, dt, than the slow ones which are integrated every $\Delta t = i$dt, with i being an integer number. In all simulation runs of this work, the small integration time step was set equal to d$t = 2$ fs and the large one to $\Delta t = 5$ dt. The duration of the MD runs varied from 40 ns for the shorter (C_{48}, C_{56}) up to 600 ns for the longer (C_{320}, C_{400}) systems. All MD runs were carried out with the large-scale atomic/molecular massively parallel simulator (LAMMPS) code[47] that can run on any parallel platform supporting the MPI library.

III. Simulation Methodology

The methodology followed in this work to efficiently simulate *cis*-1,4-PB systems with the MD method is very similar to that introduced by Harmandaris et al.[39] for linear PE. It is a three-stage approach, whereby the dynamic properties of polymer melts are calculated through (a) exhaustive EBMC simulations[41] to equilibrate the melts at all length scales, (b) atomistic MD simulations, which allow accumulating a large number of dynamical trajectories, and (c) mapping of these trajectories onto a mesoscopic model such as the Rouse and the reptation (or tube) models to extract values of the parameters describing the chain long-time dynamics. Through this, limitations

imposed by the problem of long relaxation times in a brute-force dynamic method (such as equilibrium or nonequilibrium MD) are overcome and one can get more efficiently at the dynamic and some of the rheological properties of the system. Stage (a) in particular is key to the successful implementation of the methodology since it supplies us with atomistic configurations exhaustively pre-equilibrated at all length scales, from the level of individual bonds to the level of entire chains. It relies on the application of a novel MC algorithm which, through the application of chain connectivity-altering moves, allows the system to bypass barriers limiting the natural dynamics, thus resulting in equilibration rates that are orders of magnitude faster than those realized in the dynamic simulations.[48]

As mentioned above, such a methodology has so far been followed for linear PE melts with remarkable predictions.[39] Among others, it has allowed us to consistently extract predictions for the monomer friction factor, ζ, the zero-shear rate viscosity, η_0, and the self-diffusion coefficient, D, of linear PE melts of lengths crossing over to the regime of entangled systems. New results obtained by applying the same methodology to *cis*-1,4-PB systems are presented in the next section of this paper.

IV. Results

Conformational Properties. As a check of the correctness of the MD runs, the equilibrium conformational and thermodynamic properties of the simulated *cis*-1,4-PB systems were first compared against those obtained from the EBMC runs[41] and available experimental data.[49−52] The conformation of a polymer chain can be examined in terms of bending and torsion-angle distributions, mean-square end-to-end distance, $\langle R^2 \rangle$, mean radius of gyration, $\langle R_g^2 \rangle$, and characteristic ratio, C_n.

The probability distribution of the population in the two bending angles (noted as θ_1 and θ_2 here) along a *cis*-1,4-PB chain was seen to exhibit characteristic peaks marking their equilibrium values (112° for θ_1 and 126° for θ_2) independently of chain length. As far as the distributions of the torsion angles corresponding to dihedrals φ_1 and φ_2 are concerned, these were found to be in agreement with previous simulations studies such as those of Li and Mattice,[3] Smith and Paul,[9] and the recent EBMC simulation work of Gestoso et al.[41] The distribution of dihedral ϕ_2 was seen to exhibit a maximum at around ±118° and that of ϕ_1 at ±180° and ±60° (corresponding to the trans and gauche conformational states, respectively). It was further observed that as the temperature decreases (a) the height of the two torsion-angle distributions at their peak increases (i.e., the relative population of states residing at the global minimum increases), (b) the population of the trans state (at ±180°) in the distribution of the ϕ_1 dihedral increases accompanied by an increase in the population of the two gauche states, and (c) the trans population of ϕ_2 dihedral decreases.

Figure 2 presents the time evolution of the mean-square end-to-end distance, $\langle R^2 \rangle$, of the C_{240} and C_{400} *cis*-1,4-PB melts at $T = 413$ K. Following a short initial equilibration period, $\langle R^2 \rangle$ in both cases fluctuates around a constant (or plateau) value, indicative of a fully equilibrated system. Results for $\langle R^2 \rangle$ for all systems employed in the simulations are presented in Table 3. From the simulation results for $\langle R^2 \rangle$, the characteristic ratio, C_n, for an n_{mer} monomer unit long chain can be calculated through $C_n = (\langle R^2 \rangle / 4 n_{mer} \bar{l}^2)$, where n_{mer} is the average number of monomers per chain in the simulated system and $\bar{l}^2$ is the average square skeletal bond. Plots of C_n as a function of the inverse number of monomers along the chain for the simulated *cis*-1,4-PB systems are presented in Figure 3. By extrapolating a linear fit to the data of Figure 3 to intersect the C_n axis, the characteristic ratio at infinite chain length, C_∞, can also be extracted. The value obtained from our NPT MD simulations is $C_\infty = 4.8 \pm 0.5$. This agrees remarkably well with the value of 4.9 ± 0.2 reported by Hadjichristidis et al.[51] from measurements of *cis*-1,4-PB chain dimensions in a Θ solvent and with the experimental data of Moraglio[50] and Abe and Fujita.[49] The corresponding value reported by Gestoso et al.[41] from EBMC simulations with a fixed bond-length and bond-angle force field is 4.7 ± 1.0.

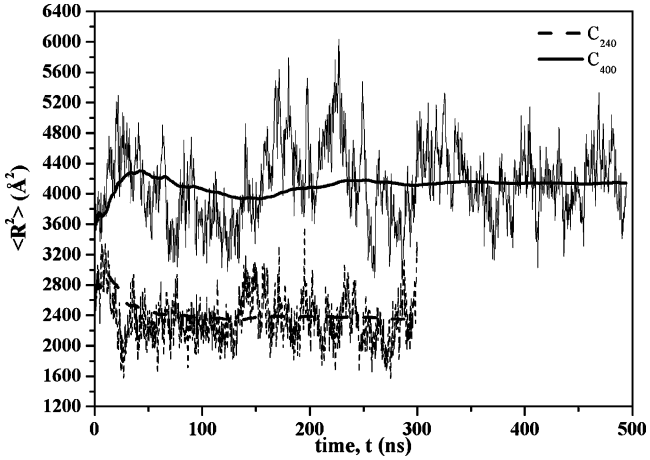

Figure 2. Time evolution of the mean-square end-to-end distance, $\langle R^2 \rangle$, for the C_{240} and C_{400} *cis*-1,4-PB systems. The lines denote the running average values [$T = 413$ K, $P = 1$ atm].

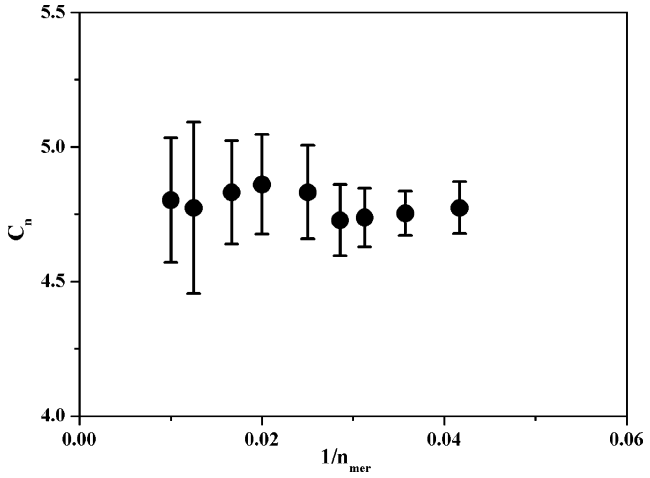

Figure 3. Values of the characteristic ratio, C_n, as a function of the inverse number of monomers, n_{mer}, along the chain from the present MD simulations [$T = 413$ K, $P = 1$ atm].

Table 3. Values of the Mean-Square End-to-end Distance, $\langle R^2 \rangle$, and Mean-Square Radius of Gyration, $\langle R_g^2 \rangle$, for the Simulated *cis*-1,4-PB Systems [$P = 1$ atm, $T = 413$ K]

system	$\langle R^2 \rangle$ (Å^2)	$\langle R_g^2 \rangle$ (Å^2)	system	$\langle R^2 \rangle$ (Å^2)	$\langle R_g^2 \rangle$ (Å^2)
C_{32}	270 ± 10	45 ± 5	C_{128}	1335 ± 30	215 ± 18
C_{48}	440 ± 10	70 ± 5	C_{140}	1430 ± 40	234 ± 18
C_{56}	530 ± 10	85 ± 7	C_{160}	1640 ± 60	257 ± 25
C_{64}	600 ± 15	95 ± 10	C_{200}	2100 ± 80	304 ± 20
C_{80}	790 ± 30	125 ± 10	C_{240}	2480 ± 100	401 ± 30
C_{96}	950 ± 20	152 ± 16	C_{320}	3100 ± 200	576 ± 30
C_{112}	1150 ± 20	184 ± 15	C_{400}	4138 ± 100	678 ± 30

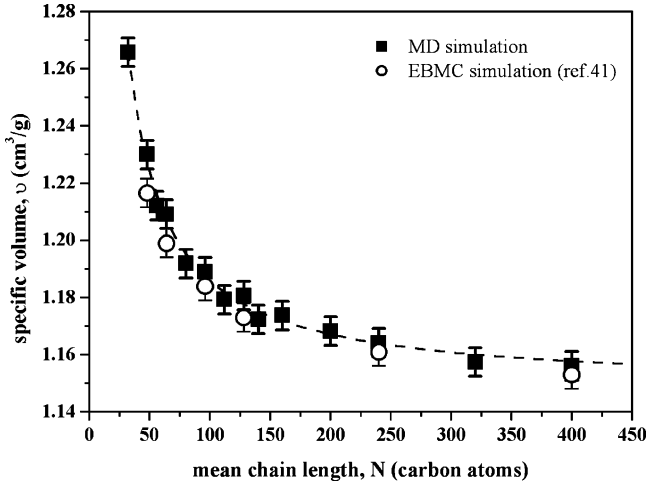

Figure 4. Dependence of the specific volume, v, on mean chain length, N, as predicted by our MD simulation runs (filled symbols) and EBMC simulations[41] (open symbols). The dashed line is a hyperbolic fit (eq 5) to the simulation data [$T = 413$ K, $P = 1$ atm].

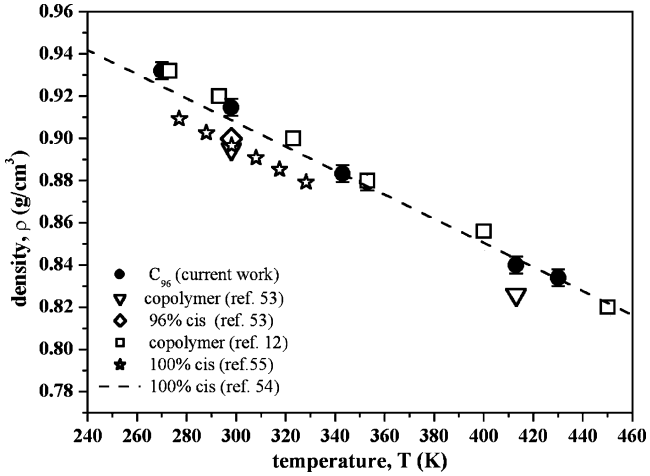

Figure 5. Temperature dependence of the density as obtained from the present MD simulations with the C_{96} system at $P = 1$ atm (filled circles) and from the MD simulations of ref 12 (open squares). Also shown are available experimental data (open triangles, open diamonds, stars, dashed line) taken from refs 53−55.

Thermodynamic Properties. Figure 4 presents the variation of the specific volume, v, of the systems studied in this work with average chain length (filled symbols), at $T = 413$ K. Also shown in the figure are a few data (open symbols) borrowed from ref 41 with a fixed bond-length and bond-angle model; these are seen to be systematically smaller from the predictions of the flexible model by about 1%. Figure 4 reveals that in *cis*-1,4-PB systems, in accordance with other polymeric systems, v decreases monotonically with increasing chain length; at high enough chain lengths, however, v attains a chain-length-independent value indicative of a true polymeric behavior. The relation between v and average chain length, N, is usually described in the literature by a hyperbolic equation

$$v = v_\infty + \frac{v_0}{N} \tag{5}$$

where v_∞ is the specific volume at infinite chain length and v_0 is a proportionality constant describing the rate with which v decreases with increasing chain length. Fitting the data of Figure 4 with eq 5, we obtain: $v_\infty = 1.147$ cm^3 g^{-1} and $v_0 = 3.806$ cm^3 g^{-1}. To compare these values to available experimental measurements, we have made use of the empirical Tait equation of state proposed by Yi and Zoller[52] to fit experimental density values of a 1,4-PB system containing only 40% cis and a small portion of 1,2-vinyl contents at 0 atm:

$$v(T) = 1.1004 + 6.718 \times 10^{-4}T + 6.584 \times 10^{-7}T^2 \text{ cm}^3 \text{ g}^{-1} \tag{6}$$

with T in °C. The value predicted from the above empirical equation for the specific volume at $T = 413$ K is $v = 1.194$ cm^3 g^{-1}, which is 4% higher than the value of v_∞ predicted from the present MD simulations.

Figure 5 shows how the density of the C_{96} *cis*-1,4-PB system varies with temperature. Also shown in the figure are (a) experimental values reported for 1,4-PB samples with a considerably larger molecular weight containing cis, trans, and vinyl conformations of the double bond,[53] (b) experimental data obtained with samples containing only cis conformations,[54,55] and (c) results from past MD simulations[12] of a similar chain length system but of a different microstructure (composition: 40% *cis*-1,4, 50% *trans*-1,4, and 10% 1,2-vinyl). Given the differences in the chemical composition of the various samples, the quantitative agreement of all sets of data is good. The practical coincidence between the MD simulation results from the present work and from ref 12, despite the different microstructure of the model, suggests that deviations from experiment are due to the force field, rather than to the microstructure. Specifically, nonbonded interactions seem to be a little too attractive for capturing the experimental PVT behavior. Nevertheless, one can say that the model employed in the present simulations (a hybrid of Smith et al.[9] and Gee and Boyd[6]) can represent the volumetric properties of *cis*-1,4-PB systems quite well.

Structural Properties. Information about the structural characteristics of *cis*-1,4-PB is extracted from the intermolecular pair distribution function $g(r)$. Figure 6a presents the function $g(r)$ for three different systems with average chain length C_{48}, C_{96}, and C_{240}, at $T = 413$ K. The position of the first peak, reflecting the average position of the first intermolecular neighbors, is located at around 5.8 Å, while that of the second peak at around 10.3 Å. As the chain length increases, a small shift of the peak positions in $g(r)$ toward smaller distances is observed due to the higher density, which coincides with the findings of ref 41. The effect of temperature on the structure of the *cis*-1,4-PB melts is depicted in Figure 6b presenting the function $g(r)$ for the C_{48} system at two different temperatures, $T = 298$ K and $T = 413$ K. The shift of the first peak toward larger distances as the temperature increases reflects the thermal expansion.

The Fourier transform of the total pair distribution function leads to the calculation of the static structure factor, $S(q)$, a quantity measured by X-ray or neutron diffraction experiments. In this way, the calculation of $S(q)$ from atomistic simulations leads to a direct comparison of the simulation results with experimental measurements. To extract $S(q)$ from our MD simulations, it was necessary to introduce hydrogen atoms at their correct positions along the chain backbone. Following ref 11, hydrogen atoms attached to the carbon atoms participating in the double bond were placed along the bisector of the double and allyl bonds, while

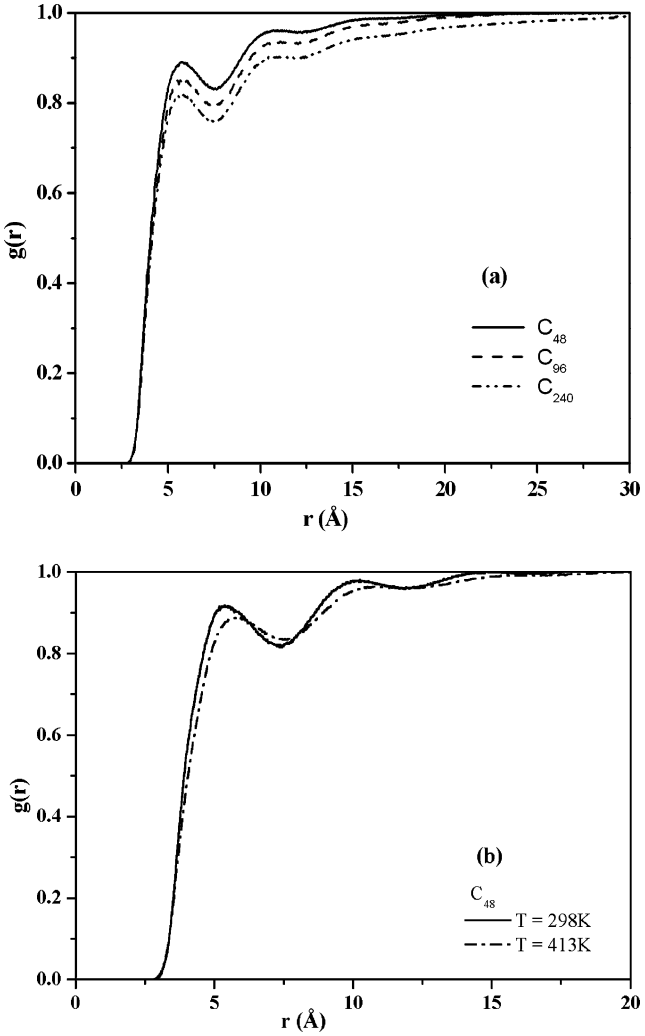

Figure 6. (a) Intermolecular pair distribution function, $g(r)$, obtained from the present MD simulations with the C_{48}, C_{96}, and C_{240} systems [$T = 413$ K, $P = 1$ atm]. (b) Intermolecular pair distribution function, $g(r)$, obtained from the present MD simulations with the C_{48} system at $T = 298$ and 413 K [$P = 1$ atm].

hydrogens participating in the methyl units were placed such that the bisector of the H−C−H angle was in the plane formed by the three carbon atoms. The value of the C−H bond length was set equal to 1.08 Å, and that of the H−C−H angle in each methyl group equal to 106.6°. To account for the different species (hydrogens and carbons) present in our systems, the static structure factor, $S(q)$, was calculated from the Fourier transform of the $H(r)$ function[56] defined through

$$H(r) = \sum_{i=1}^{2}\sum_{j=1}^{2} \frac{x_i x_j f_i f_j}{(\sum_{i=1}^{2} x_i f_i)^2} (g_{ij}(r) - 1) \qquad (7)$$

where x_i and x_j denote the number fraction of i-type and j-type atoms and f_i and f_j the respective scattering factors. Furthermore, to compare with experimental results where usually deuterated polybutadiene samples are used,[34−35,57] the scattering length used in eq 7 was that of deuterium.

The plots of $S(q)$ obtained from our simulations with the C_{140} system at $T = 298$ K and $T = 413$ K are shown in Figure 7a. Experimentally obtained $S(q)$ curves[34] at

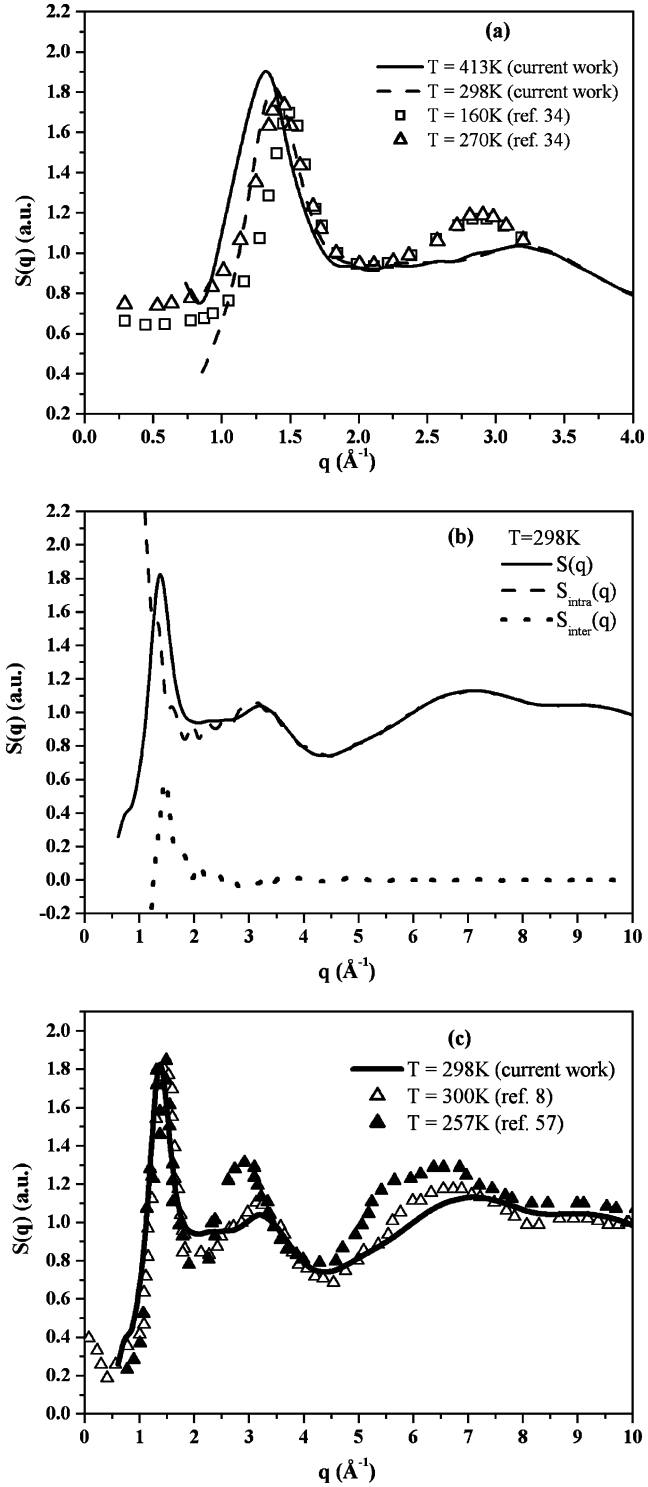

Figure 7. (a) Patterns of the static structure factor, $S(q)$, of *cis*-1,4-PB systems as obtained from the present MD simulations ($P = 1$ atm) at $T = 298$ K (dashed line) and $T = 413$ K (solid line). Also shown by the symbols are the experimental data of ref 34 obtained at $T = 160$ K (squares) and $T = 270$ K (triangles). (b) Intramolecular and intermolecular contributions to the total structure factor $S(q)$ at $T = 298$ K. (c) Patterns of the static structure factor, $S(q)$, over a wider range of q values. The solid line corresponds to the results of the present MD simulation study at $T = 298$ K ($P = 1$atm), the open symbols show the pattern obtained from the MD simulation work of ref 8 at $T = 300$ K, and the filled symbols are the experimental data of ref 57.

160 and 270 K are also presented in Figure 7a, demonstrating a satisfactory agreement with the pattern

obtained from the simulations. Both sources of data support the existence of (a) a sharp peak at about 1.4 $Å^{-1}$ and (b) a diffuse (broader) peak at around 3 $Å^{-1}$. Figure 7b presents the intra- and intermolecular contributions to the total structure factor at $T = 298$ K. It is obvious that the first peak at 1.4 $Å^{-1}$ reflects both intra- and intermolecular correlations, while the second one reflects intrachain correlations. In agreement with experimental observations,[35] our results also reveal a shift of the first peak toward lower q values as the temperature increases; in contrast, the temperature does not seem to affect appreciably the location of the second peak. This can be seen more clearly in Figure 7c where $S(q)$ is shown for q values larger than those reported in Figure 7a. Two more sets of data are shown in Figure 7c corresponding to (a) an experimental estimation of the $S(q)$ pattern (represented by the filled triangles) with a sample containing trans, cis, and vinyl contents[57] and (b) a calculation of the $S(q)$ pattern by Okada et al.[8] through MD simulations (represented by the open triangles) with a *cis*-1,4-PB system of a single chain made up of 200 monomers at $T = 300$ K. The differences dictated between the experimental (on one hand) and the MD simulation (on the other hand) data should be mainly attributed to the different microstructure of the sample used in the measurements. To explain, in particular, the clear difference seen in the position and shape of the second peak at around 3 $Å^{-1}$ between simulation and experiment, we carried out an NPT MD simulation with a relatively short *trans*-1,4-PB system. Indeed, the position of the peak was seen to shift to the left, thus better matching the experimental pattern. Differences between simulation and experiment in the height of the second peak reflect most probably differences in intramolecular correlations along the PB chain and were also present in the simulation with the *trans*-1,4-PB melt.

Local Dynamics. The local dynamics of the *cis*-1,4-PB chains, particularly their torsional dynamics, is studied in terms of the torsional autocorrelation function (TACF) defined as

$$P(\phi(t)) = \frac{\langle \cos(\phi(t)\cos(\phi(0))\rangle - \langle(\cos(\phi(0))\rangle^2}{\langle \cos(\phi(0)\cos(\phi(0))\rangle - \langle(\cos(\phi(0))\rangle^2} \quad (8)$$

The relaxation of the two $P(\varphi(t))$ curves corresponding to the ϕ_1 and ϕ_2 dihedrals along a *cis*-1,4-PB chain as obtained from our MD simulations with the C_{96} system at four different temperatures is shown in parts a and b of Figure 8; Figure 9 shows how the $P(\phi_1(t))$ curves decay in time as a function of the system chain length. The simulation data show that (a) as the temperature increases, the decay of both TACF's to zero is accelerated and (b) the chain local dynamics is for all practical purposes independent of the system chain length. Also shown by the symbols in Figure 8a are the best fits to the $P(\phi_1(t))$ TACF for the C_{96} system at $T = 298$ K (circles) and $T = 413$ K (squares) with a stretched exponential or KWW function of the form:[58]

$$P(\phi(t)) = \exp(-(t/\tau_{KWW})^{\beta_\phi}) \quad (9)$$

which is seen to follow the corresponding curve remarkably closely. Similar accurate fits were observed for the $P(\phi_1(t))$ and $P(\phi_2(t))$ TACFs of all simulated systems. The values obtained for the characteristic time, τ^{ϕ}_{KWW}, the stretching exponent, β^{ϕ}, and the correlation time, τ^{ϕ}_{c}, calculated through $\tau_c = \tau_{KWW}((\Gamma(1/\beta)/\beta))$ are reported in Table 4; also reported in Table 4 is the variation of τ^{ϕ}_{KWW}, β^{ϕ} and τ^{ϕ}_{c} with T. The following conclusions can be drawn from the entries of the table: (a) the angle ϕ_1 (describing the torsion of the bond connecting successive

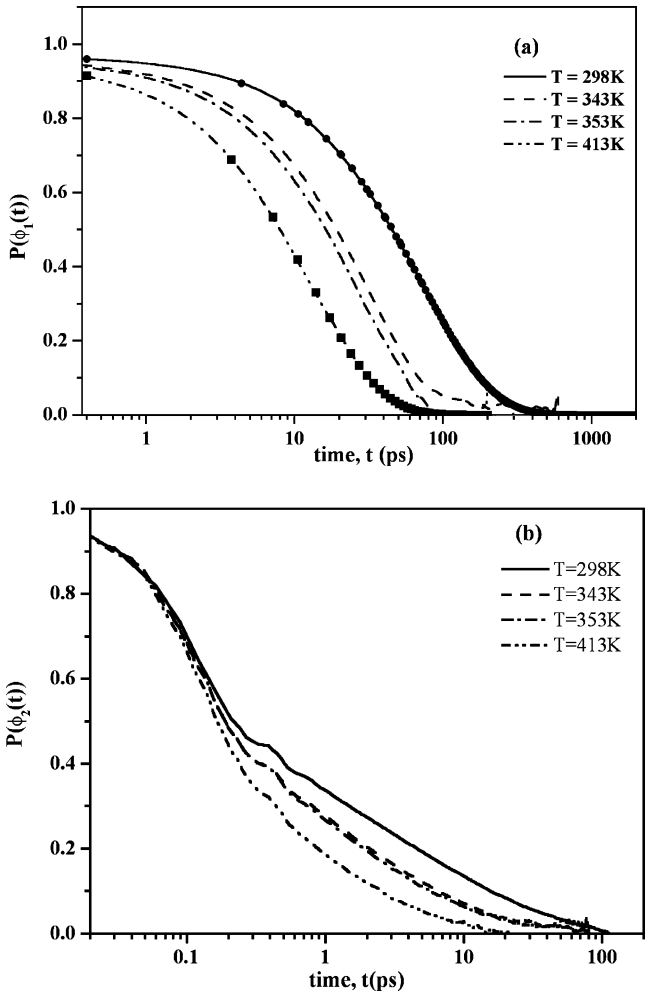

Figure 8. Time autocorrelation functions for: (a) the ϕ_1 and (b) the ϕ_2 torsion angles, as obtained from the present MD simulations with the C_{96} system, at four different temperatures (298, 343, 353, and 413 K). The symbols (circles and squares) correspond to the best KWW fits (see eq 9) of the curves at $T = 298$ K and $T = 413$ K [$P = 1$ atm].

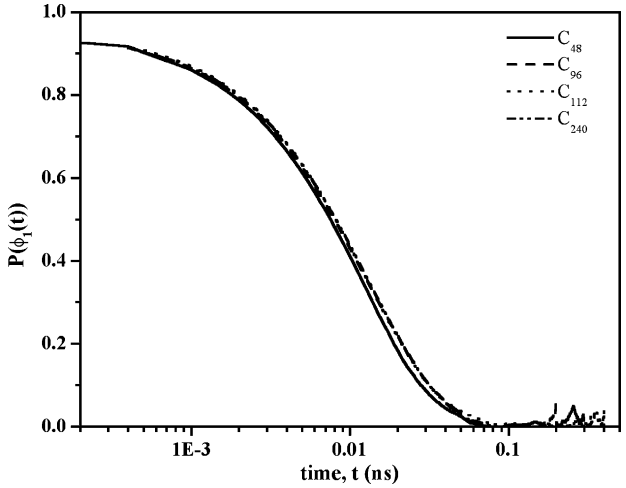

Figure 9. Time autocorrelation functions for the ϕ_1 torsion angles, as obtained from the present MD simulations with the C_{48}, C_{96}, C_{112}, and C_{240} systems [$T = 413$ K, $P = 1$ atm].

Table 4. Values of the Characteristic Kohlrausch-Williams Watts Relaxation Times, τ^{ϕ}_{KWW}, Stretching Exponents, β^{ϕ}, and Correlation Times, τ^{ϕ}_{c}, of the KWW Functions Employed to Fit the Time Autocorrelation Functions of the ϕ_1 and ϕ_2 Torsional Angles, as a Function of Temperature [P = 1 atm]

	ϕ_1		
T (K)	$\tau^{\phi_1}_{KWW}$ (ps)	β^{ϕ_1}	$\tau^{\phi_1}_{c}$ (ps)
298	68.7	0.87	73.7
343	28.2	0.85	30.68
353	23.6	0.89	24.9
413	12.1	0.86	13.1
430	10.11	0.88	10.77
	ϕ_2		
T (K)	$\tau^{\phi_2}_{KWW}$ (ps)	β^{ϕ_2}	$\tau^{\phi_2}_{c}$ (ps)
298	0.88	0.30	8.15
343	0.48	0.31	3.85
353	0.44	0.32	3.09
413	0.30	0.33	1.87
430	0.27	0.33	1.56

monomers along a *cis*-1,4-PB chain) relaxes more slowly than the angle ϕ_2 (describing the torsion of the allyl bonds), (b) the value of the stretching exponent β^{ϕ} characterizing the dynamics of dihedral ϕ_2 is significantly smaller than that characterizing the dynamics of ϕ_1, and (c) for all practical purposes, the value of β^{ϕ} can be assumed to be independent of the system temperature. It is also interesting to note that, although ϕ_2 exhibits a larger cooperativity (lower β^{ϕ}) than ϕ_1, it decorrelates much faster than ϕ_1. A similar trend characterizes the relaxation of the different torsion angles in PI.[59] The reason for this is that the torsion angle ϕ_2, next to the double bond, is characterized by a faster initial decay due to significant librations caused by rather wide potential wells. On the other hand, the torsion autocorrelation function for the angle ϕ_1, associated with the bond connecting two monomers, displays very small amplitudes for librations, resulting in a much longer mean correlation time.

Terminal Relaxation Properties. Figure 10 presents the decay of the orientational autocorrelation function for the end-to-end vector $\langle \mathbf{R}(t)\cdot\mathbf{R}(0)\rangle/\langle R^2\rangle$ as a function of time for the longest simulated melts (C_{160}, C_{200}, C_{320}, and C_{400}) at T = 413 K. The rate at which $\langle \mathbf{R}(t)\cdot\mathbf{R}(0)\rangle/\langle R^2\rangle$ approaches the zero value is a measure

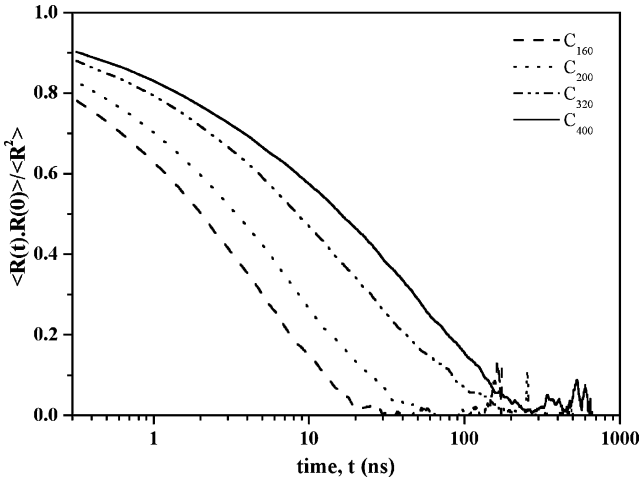

Figure 10. Time autocorrelation function for the chain end-to-end vector, $\langle \mathbf{R}(t)\cdot\mathbf{R}(0)\rangle/\langle R^2\rangle$, for the C_{160}, C_{200}, C_{320}, and C_{400} systems [T = 413 K, P = 1 atm].

of how fast the chain "forgets" its initial configuration, i.e., of the rate of the overall chain relaxation. The figure clearly demonstrates that the function $\langle \mathbf{R}(t)\cdot\mathbf{R}(0)\rangle/\langle R^2\rangle$ eventually drops to zero for all simulated systems (even for the longest C_{400}). It also nicely demonstrates that the time needed for the function $\langle \mathbf{R}(t)\cdot\mathbf{R}(0)\rangle/\langle R^2\rangle$ to reach zero increases rapidly with increasing chain length.

To quantify the long-time dynamics of the simulated *cis*-1,4-PB melts, we first attempted to fit the $\langle \mathbf{R}(t)\cdot\mathbf{R}(0)\rangle/\langle R^2\rangle$-vs-$t$ curves for some of the shorter-chain-length systems with the Rouse model, according to which:

$$\frac{\langle \mathbf{R}(t)\cdot\mathbf{R}(0)\rangle}{\langle R^2\rangle} = \sum_{p=1,3,..} \frac{8}{p^2\pi^2} \exp\left(-\frac{t}{\tau_p}\right) \qquad (10)$$

In eq 10, τ_p denotes the spectrum of relaxation times:

$$\tau_p = \frac{\tau_1}{p^2} \qquad (11)$$

with τ_1 being the longest relaxation time, equal to

$$\tau_1 = \frac{\zeta N\langle R^2\rangle}{3\pi^2 k_B T} \qquad (12)$$

Parts a and b of Figure 11 show how the time autocorrelation functions for the end-to-end vector obtained directly from the present NPT MD simulations for the C_{112} and C_{400} *cis*-1,4-PB melts at T = 413 K compare to their best fits obtained with the Rouse model expression, eq 10, keeping the first five Rouse modes (p = 1, 3, 5, 7, and 9) in the sum. Also shown in Figure 11a,b are the best fits to the simulation curves with stretched exponential (or KWW) functions of the form described by eq 9. It is seen that the Rouse model does not provide a satisfactory description of the simulation data, even for the shorter C_{112} melt: the best fit fails to follow the fast initial drop of the curve; furthermore, it cannot describe accurately enough the slowly decaying part of the curve at long times (terminal regime). Similar deviations from the Rouse dynamics have been reported in past MD simulations[11,13] of a 1,4-PB system at T = 353K. In contrast, the KWW fits are much more satisfactory: they can faithfully follow the predicted $\langle \mathbf{R}(t)\cdot\mathbf{R}(0)\rangle/\langle R^2\rangle$-vs-$t$ curves over the entire time scale, even for the longest systems studied in this work, C_{400} (see Figure 11b).

The values obtained for the characteristic relaxation time, τ_{KWW}, the stretching exponent, β, and the correlation time (integral under curve), τ_c (calculated through $\tau_c = \tau_{KWW}(\Gamma(1/\beta)/\beta)$), describing the terminal relaxation of all *cis*-1,4-PB melts simulated here are listed in Table 5. The dependence of τ_c on average chain length is graphically shown in Figure 12 on a log−log plot. The variation of the two relaxation times with temperature is included in Table 6. The following conclusions can be drawn from the entries of Tables 5 and 6 and the data sets of Figure 12: (a) the same value of the stretching exponent, β, in the interval [0.51, 0.76] practically characterizes the terminal dynamics of the end-to-end vector of all *cis*-1,4-PB systems independently of their molecular length and temperature, (b) a change is observed in the slope of the τ_c-vs-N curve at around N = 200 marking the passage to the entangled regime, and (c) the τ_c-vs-N curve can be described quite ac-

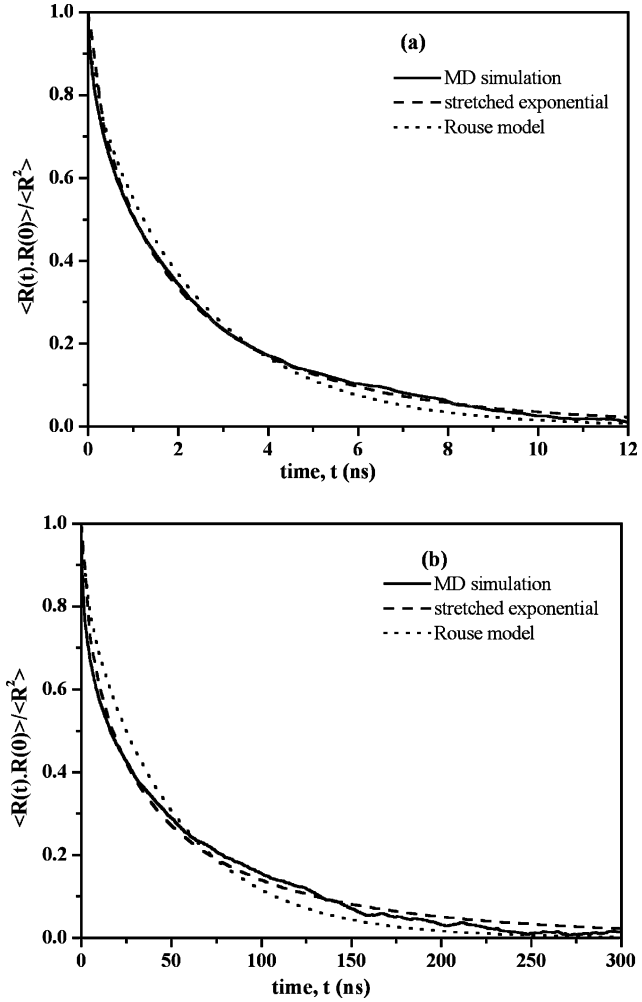

Figure 11. Time autocorrelation function for the chain end-to-end vector for the C_{112} (a) and C_{400} (b) systems at $T = 413$ K as obtained from the MD simulations (solid line) and as predicted from the Rouse model through eq 10 using only the first five Rouse modes (dotted line). The dashed line depicts the best KWW (see eq 9) fits to the simulated time autocorrelation functions.

Table 5. Values of the Characteristic Relaxation Time, τ_{KWW}, Stretching Exponent, β, and Correlation Time, τ_c, Describing the Terminal Relaxation of the Simulated *cis*-1,4-PB Systems [$T = 413$ K and $P = 1$ atm]

N	τ_{KWW} (ns)	β	τ_c (ns)	N	τ_{KWW} (ns)	β	τ_c (ns)
32	0.10	0.71	0.12	128	2.18	0.52	3.09
48	0.28	0.74	0.34	140	2.85	0.68	3.71
56	0.35	0.66	0.50	160	3.68	0.66	4.94
64	0.39	0.63	0.53	200	5.28	0.60	7.48
80	0.69	0.71	0.87	240	8.84	0.51	17.06
96	1.05	0.60	1.58	320	20.05	0.55	34.05
112	1.75	0.68	2.28	400	36.75	0.60	55.31

curately with a power law of the form $\tau \propto M^b$ (or $\tau_c \propto M^b$) with $b \approx 2.1$ for $N < 160$ and $b \approx 2.8$ for $N > 200$. Remarkably, both of these dependencies are close to those suggested by the analytical Rouse (where $b = 2$) and reptation models (where $b = 3$) for the corresponding Rouse and disengagement times, respectively.[14] However, the transition from Rouse to reptation dynamics is not sharp. Simulations with significantly longer PB systems are needed to track the transition regime more faithfully.

Self-Diffusion Coefficient, *D*. Significant information about the long-time dynamics of the simulated *cis*-1,4-PB systems is provided by the dependence of the chain self-diffusion coefficient, D, on chain length. D is readily calculated in an MD simulation from the linear part of the mean-square displacement (msd) of the chain center-of-mass with respect to time through the Einstein relation. Typical plots of the chain center-of-mass msd $\langle(R_{cm}(t) - R_{cm}(0))^2\rangle$ in time for the longest *cis*-1,4-PB systems simulated in this work (C_{240}, C_{320}, C_{400}) at $T = 413$ K are shown in Figure 13. Similar plots are obtained with the rest of the systems.

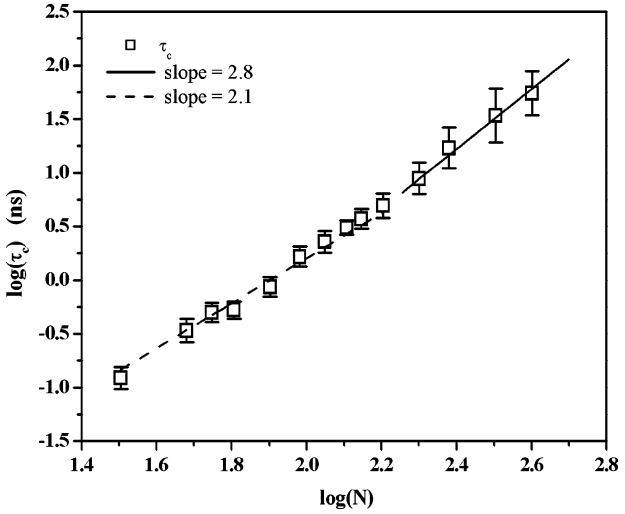

Figure 12. Dependence of the characteristic relaxation time, τ_c, on chain length, N, on a log−log plot. The lines depict the best linear fits to the function $\tau_c = \tau_c(N)$. The resulting slopes are 2.1 for chain lengths N less than about C_{200} and 2.8 for chain lengths N above C_{200} [$T = 413$ K, $P = 1$ atm].

Figure 14 presents the dependence of D on average chain length, N (or molecular weight, M), in a log−log plot, at $T = 413$ K. Three distinct regions appear in the figure: (a) For $N < 80$, D follows a power law dependence, $D \approx N^{-b}$ with $b > 1$, indicative of a chain motion dominated by chain end effects; the latter can be described through the free volume theory.[60,61] (b) For systems with $80 < N < 160$, $D \approx N^{-b}$ with $b \cong 1$, i.e., the chain motion is approximately Rouse-like[14,15] (the solid line in Figure 14 corresponds to a line with slope exactly equal to −1). (c) For systems with $N \geq 200$, D decreases more rapidly with increasing chain length and $D \approx N^{-b}$ with $b \approx 2.1$. Despite that the transition from Rouse to reptation dynamics is not sharp, for high enough chain lengths, reptation seems to dominate system dynamics, causing a slowing down of the overall chain motion. The value $b = 2.1$ for the exponent predicted from our simulations is somewhat larger than the value $b = 2$ suggested by the original reptation theory, but it is close to that predicted by the modified reptation theory,[24] which takes into account contour length fluctuations (CLF) and constraint release (CR) phenomena, according to which, b should be between 2.2 and 2.3; these phenomena should be important for the relatively short chain lengths examined here. These exponents agree also with other simulation[39] and experimentally[32,38] measured data with different polymer melts that support a value of b between 2.2 and 2.4. Figure 14 shows further that, in *cis*-1,4-PB, the critical molecular weight where the crossover of D from the Rouse to the reptation regime takes place is a little higher than in linear PE (compare Figure 14 with Figure 2 of ref 39). This suggests that *cis*-1,4-PB should be characterized by M_e and M_c values larger than those of linear PE, which agrees with available literature

Table 6. Values of the Characteristic Relaxation Time, τ_{KWW}, Stretching Exponent, β, and Correlation Time, τ_c, Describing the Terminal Relaxation of the C_{48}, C_{80}, C_{96}, and C_{140} *cis*-1,4-PB Systems at Different Temperatures [P = 1 atm]

	N											
	48			80			96			140		
T (K)	τ_{KWW} (ns)	β	τ_c (ns)	τ_{KWW} (ns)	β	τ_c (ns)	τ_{KWW} (ns)	β	τ_c (ns)	τ_{KWW} (ns)	β	τ_c (ns)
298	0.96	0.76	1.14	4.33	0.76	5.10	6.47	0.58	10.2	15.6	0.67	20.6
343	0.48	0.66	0.64	1.75	0.71	2.30	2.73	0.63	3.87			
353	0.41	0.67	0.54	1.74	0.71	2.16	2.08	0.65	2.84	5.40	0.75	6.43
413	0.28	0.74	0.34	0.69	0.71	0.86	1.05	0.60	1.58	2.85	0.68	3.71
430	0.20	0.72	0.25				0.99	0.65	1.35	2.22	0.61	3.27

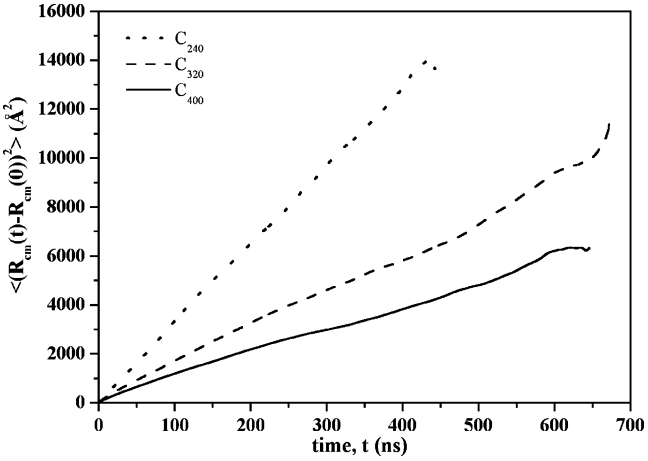

Figure 13. The mean-square displacement (msd) of the chain center-of-mass as a function of time for the simulated C_{240} (dotted), C_{320} (dashed), and C_{400} (solid line) systems [T = 413 K, P = 1 atm].

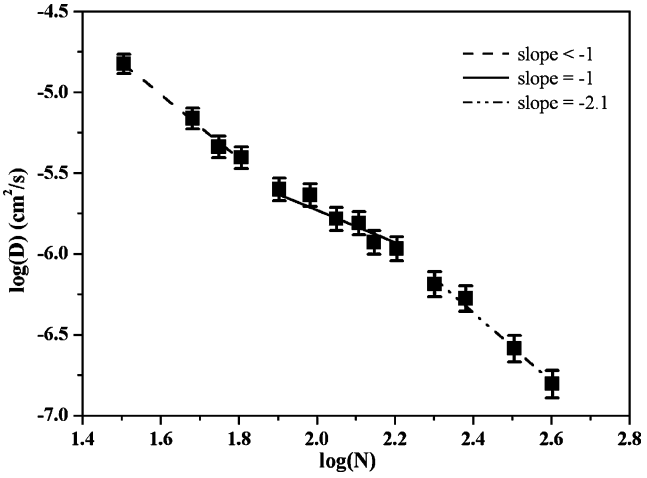

Figure 14. Dependence of the self-diffusion coefficient, D, on mean chain length, N, on a log−log plot as obtained from the present MD simulations [T = 413 K, P = 1 atm].

data[53] according to which the molecular weight between entanglements, as extracted from the plateau modulus, is M_e = 1750−2200 g mol^{-1} for *cis*-1,4-PB and M_e = 1200 g mol^{-1} for linear PE.

To directly compare our MD-based D values with results obtained from other simulation studies and NSE experiments,[11] we also simulated a 40-chain C_{96} *cis*-1,4-PB system at T = 353 K, characterized by the same polydispersity index, I, as the experimental sample (I = 1.05); the value of D obtained was 11.5 × 10^{-7} cm^2 s^{-1}, which is considerably higher than that reported in ref 11. However, it should be mentioned that the samples measured in the NSE experiments had a different microstructure (40% *cis*-1,4, 50% *trans*-1,4, and

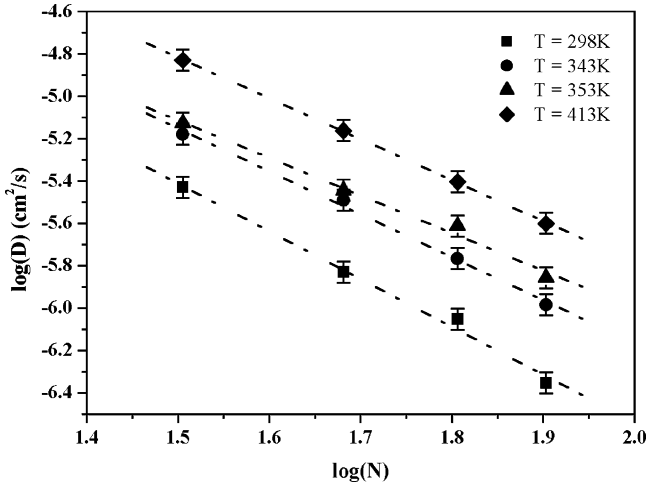

Figure 15. Self-diffusion coefficient, D, as a function of mean chain length, N, as obtained from the present MD simulations with the C_{32}, C_{48}, C_{64}, and C_{80} *cis*-1,4-PB systems, at T = 298 K (squares), T = 343 K (circles), T = 353 K (triangles), and T = 413 K (diamonds). The slope of the dashed lines changes from −2.25 at T = 298 K to −1.7 at T = 413 K. In all cases, P = 1 atm.

10% 1,2-vinyl content) and a longer chain length (114 carbon atoms per chain) than the system simulated here. The values of D reported for the samples used in the NSE experiments of ref 11 are a factor of 4 smaller than the value obtained here with the C_{96} system. A better quantitative agreement is observed between our results and the simulation data of ref 11 for the shorter system (containing 100 carbon atoms per chain) with microstructure 50% *cis*-1,4 and 50% *trans*-1,4: for this system, the reported value is only two times smaller than the one extracted here.

The dependence of diffusivity on temperature is shown in Figure 15 which presents D-vs-N plots for the shorter-chain systems (C_{32}, C_{48}, C_{64}, and C_{80}) at different temperatures in a log−log plot. It is seen that the exponent b (in the $D \approx N^{-b}$ scaling law) varies from 1.7 at T = 413 K to 2.25 at T = 298 K. Similar results for the temperature dependence of b have been presented in atomistic MD simulations of monodisperse *n*-alkanes and *cis*-1,4-polyisoprene oligomer melts.[61] To quantify the temperature dependence of D, Figure 16 presents Arrhenius plots of the chain self-diffusion coefficient (i.e., plots of D as a function of the inverse temperature, 1/T) for the C_{48} (squares), C_{96} (circles), and C_{140} (triangles) *cis*-1,4-PB systems. From the slope of the corresponding curves, one can obtain estimates of the apparent activation energy, E_a^{app}:

$$E_a^{app} = -\frac{R}{0.434}\frac{\partial(\log D)}{\partial(1/T)} \qquad (13)$$

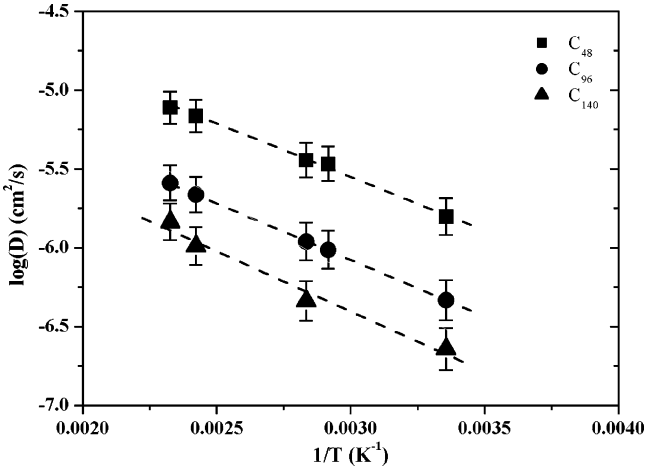

Figure 16. Dependence of the chain center-of-mass self-diffusion coefficient, D, on temperature, T, as obtained from the present MD simulations with the C_{48} (squares), C_{96} (circles), and C_{140} (triangles) systems. In all cases, $P = 1$ atm.

It is seen that E_a^{app} rises from 3.0 kcal mol^{-1} for the C_{48} system to 3.5 kcal mol^{-1} for the C_{140} system. Unfortunately, no experimental data are available in the literature with which to compare E_a^{app} for *cis*-1,4-PB.

Friction Coefficient, ζ. Following the methodology outlined in ref 39, the simulation data for the chain self-diffusion coefficient, D, can be mapped onto results for the friction factor, ζ. For short-chain-length systems, this is achieved by making use of the Rouse model according to which $N\zeta = (k_BT/D)$. On the other hand, if the mapping is done through the reptation theory, then $N\zeta = (k_BT/3D)\,(\alpha^2/\langle R^2\rangle)$, which shows that one needs to calculate also the tube diameter, α. This can be accomplished by the iterative procedure introduced in ref 39 that leads to the calculation of α through a novel projection of chain conformations onto their primitive paths and a self-consistent mapping of the msd of the primitive path points extracted from the MD simulations onto the analytical expression proposed by reptation theory.

The projection of chain conformations to primitive paths is realized through a projection operation involving a single parameter, ξ, which governs the stiffness of the chain in the coarse-grained (primitive path) representation. The parameter ξ is mathematically defined as the ratio of the constants of two types of Hookean springs: The first type connects adjacent beads within the projected primitive path, and the second type connects the projected beads of the primitive path with the corresponding atomistic units.[40] Different values of ξ lead to different parametrizations, i.e., to different primitive paths and, consequently, to different values of the contour length, L. Once a value for ξ has been chosen, the primitive path is fully defined which allows calculating the tube diameter α through $La = \langle R^2\rangle$.The proper ξ value is found by following a self-consistent scheme based on the msd of the primitive path points and by comparing the resulting curve to that obtained from the reptation theory for times $t < \tau_d$, where τ_d is the chain disentanglement time, using the values of $\langle R^2\rangle$ and D (long-time diffusivity of the centers of mass) calculated directly from the atomistic MD simulations.[39] The entire procedure is repeated until convergence is achieved, i.e., until a ξ value is found for which the two curves coincide. Such a methodology is performed self-consistently without any additional adjustable parameters or any experimental input and allows a reliable estimation of the tube diameter, α, by utilizing atomistically collected MD data only for times shorter than τ_d. It has been applied in ref 39 to linear PE with remarkable success, and is extended here to *cis*-1,4-PB systems.

Figure 17. Atomistic snapshot of a C_{400} *cis*-1,4-PB chain and its corresponding primitive path (smoother curve) for a value of the fitting parameter, ξ, controlling the geometry of the projection equal to 50 [$T = 413$ K, $P = 1$ atm].

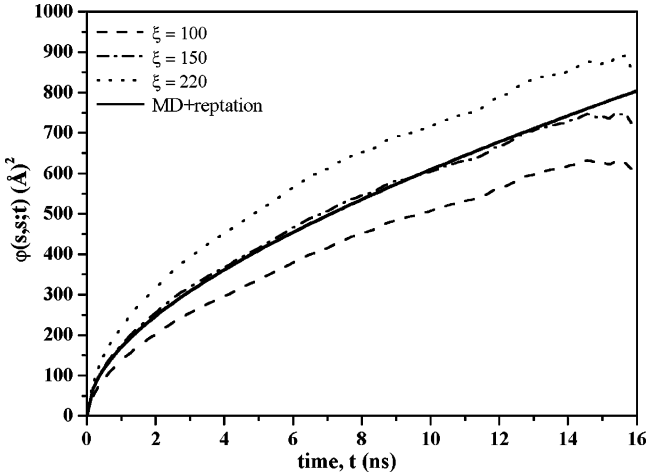

Figure 18. Mean-square displacement of the primitive path segments $\varphi(s,s;t)$ versus time as obtained by mapping the atomistic MD results onto the reptation model for different ξ values. The solid curve corresponds to the calculation of $\varphi(s,s;t)$ according to the original reptation theory [$T = 413$ K, $P = 1$ atm].

Figure 17 shows a typical plot of an atomistic *cis*-1,4-PB chain and its corresponding primitive path. Figure 18, on the other hand, presents a plot of the msd of the primitive path segments, $\varphi(s,s;t)$, versus time, t, for different values of the fitting parameter ξ controlling the geometry of the mapping from atomistic chains to primitive paths. The value of ξ which provides a consistent description of the atomistic MD data with the equations of the reptation theory is found to be $\xi = 150$. The corresponding value for the tube diameter, α, is 64

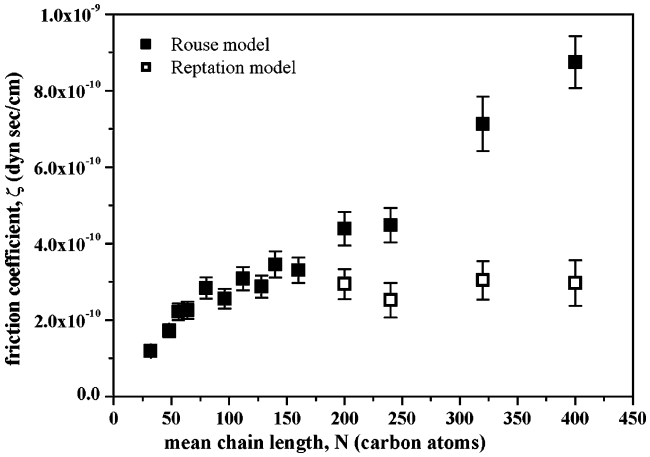

Figure 19. Values of the friction coefficient, ζ, for various chain lengths, as obtained by mapping atomistic MD data for D onto the Rouse (filled symbols) and the reptation model (open symbols) [$T = 413$ K, $P = 1$ atm].

Å. This is larger than the value of 38 Å reported experimentally for highly entangled *cis*-1,4-PB systems.[53] The deviation, which is very comparable to that seen in the case of PE,[39] should be sought in the (rather) small size of the C_{400} system used to estimate ξ. Work is currently in progress to extend the MD simulations to longer-chain-length *cis*-1,4-PB systems, such as C_{500} and C_{600}.

Figure 19 presents the values of the friction coefficient, ζ, at $T = 413$ K extracted by either mapping, and its dependence on average chain length, N. According to the classical Rouse and reptation theories, ζ should be independent of the size of the polymer chain; it should depend only on the chemical structure of the system. Similarly to what was observed for linear PE, a change in the mechanism of the dynamics is seen also for *cis*-1,4-PB at around $N = 200$, which cannot be accommodated by the Rouse model unless a chain-length-dependent ζ value is assumed. In contrast, in the long-chain regime ($N \geq 200$), the reptation model provides a consistent description of the *cis*-1,4-PB dynamics characterized by a constant (equal to $[3.0 \pm 0.2] \times 10^{-10}$ dyn s cm^{-1}), chain-length-independent ζ value per carbon atom. The reader is reminded that the results of Figure 19 are based on maps of the MD trajectory onto the classical Rouse and reptation theories without consideration of free volume (for the Rouse model) and CLF or CR effects (for the reptation model). Given the short chain lengths of the simulated systems, incorporation of CLF and CR effects would be appropriate. Computational procedures whereby this can be achieved are under development.

Dynamic Structure Factor, $S(q,t)$. The Brownian motion of polymers can be experimentally studied by techniques such as dynamic light scattering and neutron spin−echo (NSE) which allow one to extract the dynamic structure factor $S(\mathbf{q},t)$ of the melt

$$S(\mathbf{q},t) \equiv \frac{1}{N}\sum_{n,m}\langle \exp[i\mathbf{q}\cdot(\mathbf{R}_n(t) - \mathbf{R}_m(0))]\rangle \qquad (14)$$

where $\mathbf{q}$ denotes the scattering vector and $\mathbf{R}_n(t)$ the position vector of chain segment n at time t. For an isotropic melt, eq 14 simplifies to

$$S(q,t) = \frac{1}{N}\sum_{n,m}\langle \sin\,[qR_{nm}(t)]/qR_{nm}(t)\rangle \qquad (15)$$

where q is the magnitude of $\mathbf{q}$ and $R_{nm}(t)$ the magnitude of $\mathbf{R}_n(t) - \mathbf{R}_m(0)$. What is actually measured in NSE experiments is the normalized single-chain intermediate coherent dynamic structure factor $S(q,t)/S(q,0)$:

$$S'(q,t) = \frac{S(q,t)}{S(q,0)} = \frac{\sum_{n,m}\langle \sin\,[qR_{nm}(t)]/qR_{nm}(t)\rangle}{\sum_{n,m}\langle \sin\,[qR_{nm}(0)]/qR_{nm}(0)\rangle} \qquad (16)$$

$S'(q,t)$ can also be extracted from MD simulations by recording the time correlation function $\mathbf{R}_n(t) - \mathbf{R}_m(0)$ of chain segments n and m and calculating its magnitude as a function of time. This provides a means for comparing MD simulation results with experimental measurements to gain additional insight into the polymer melt dynamics. It is also important to mention that, for the Rouse model, $S(q,t)$ can be calculated rigorously:

$$S(q,t) = \frac{1}{N_k}\exp[-q^2Dt]\sum_{n,m}^{N_k}\exp\left\{-\frac{q^2b_k^2}{6}\left|n - m\right| - \frac{2q^2N_kb_k^2}{3\pi^2}\sum_{p=1}^{N_k}\frac{1}{p^2}\cos\left(\frac{p\pi n}{N_k}\right)\cos\left(\frac{p\pi m}{N_k}\right)\left[1 - \exp\left(-\frac{t}{\tau_p}\right)\right]\right\} \qquad (17)$$

where N_k denotes the number of statistical segments in the chain, b_k the statistical segment length, D the self-diffusion coefficient of the chain center-of-mass, and τ_p the spectrum of relaxation times. A similar calculation has been carried out by de Gennes[62] and Kremer and Binder[63] for the reptation model valid for wavevectors, q, such that $(1/\alpha) \gg q \gg (1/\sqrt{\langle R^2\rangle})$, where α is the tube diameter and $\langle R^2\rangle$ the equilibrium mean-square chain end-to-end distance (see eq 2 in ref 64)

$$\frac{S(q,t)}{S(q,0)} = \left\{1 - \left(\frac{q\alpha}{6}\right)^2 f\left[q^2l_p^2\left(\frac{2k_BT}{l_p^2\zeta}t\right)^{1/2}\right]\right\}\frac{8}{\pi^2}\sum_{p=1}^{\infty}\frac{1}{(2p-1)^2}\exp\left(-\frac{t(2p-1)^2}{\tau_d}\right) \qquad (18)$$

with l_p denoting the persistence length of the polymer chains and $f(u) = \exp(u^2/36)\mathrm{erfc}(u/6)$. Such an equation has been used by Faller and Müller-Plathe[64] to arrive at an estimate of the tube diameter, α, and how it depends on chain length and stiffness. Unfortunately, the chain lengths of the *cis*-1,4-PB systems investigated here are too short to satisfy $(1/\alpha) \gg (1/\sqrt{\langle R^2\rangle})$. We hope to be able to carry out such an analysis soon in conjunction with simulation data for the equilibrium dynamics of significantly longer *cis*-1,4-PB systems.

Figure 20a,b presents results for the intermediate dynamic structure factor $S(q,t)/S(q,0)$ as obtained directly from our NPT MD simulations for the C_{96} and

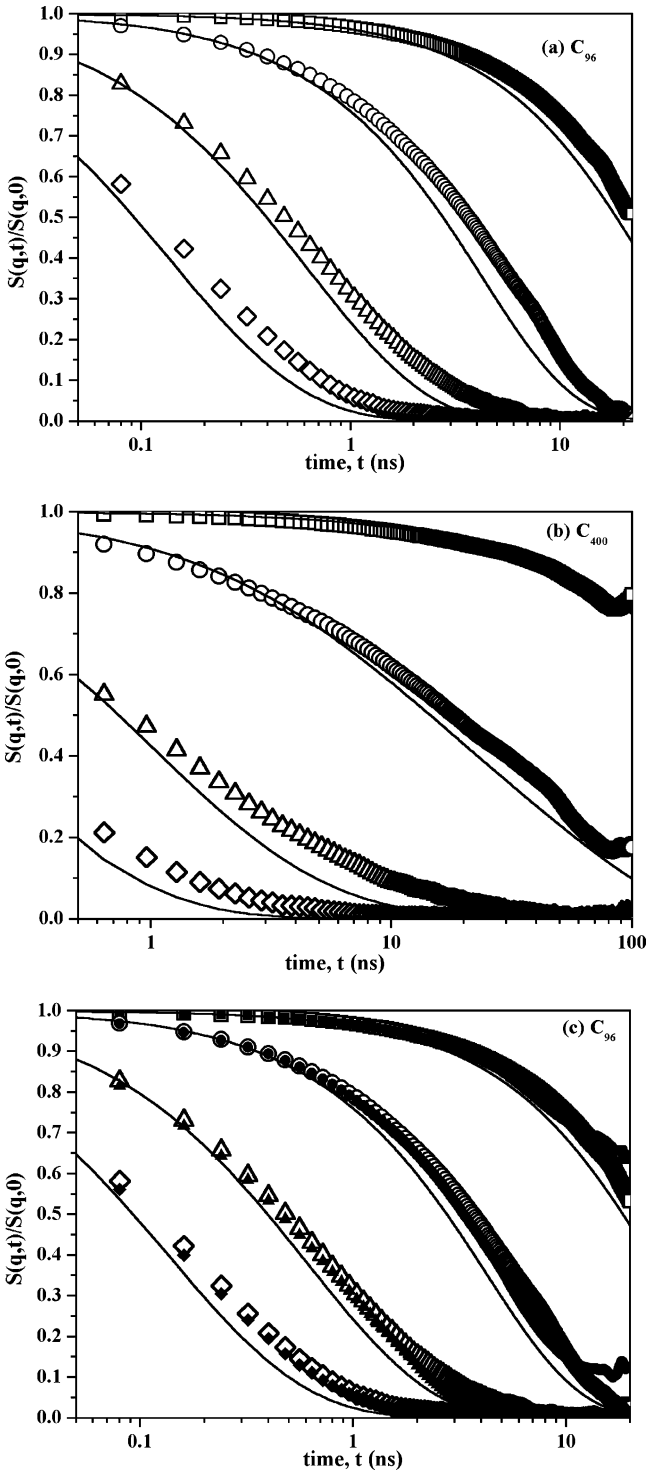

Figure 20. (a) Plots of the normalized single-chain dynamic structure factor, $S(q,t)/S(q,0)$, as obtained from the present MD simulations (symbols) for various q values (0.04, 0.10, 0.20, and 0.30 Å^{-1}) with the C_{96} *cis*-1,4-PB system [$T = 413$ K, $P = 1$ atm]. The solid line denotes the predictions of the Rouse model (see eq 17). (b) Same as Part (a) but for the C_{400} system. (c) Normalized single-chain dynamic structure factors obtained from NPT (open symbols) and NVT (filled symbols) MD simulations with the C_{96} *cis*-1,4-PB system at the same melt density [$T = 413$ K, $P = 1$ atm].

C_{400} *cis*-1,4-PB systems (symbols) using eq 16 and as calculated for the Rouse model (lines) using eq 17 for q values ranging from 0.02 to 0.30 Å^{-1}. The curves in the figure show that there exists no q value for which a satisfactory agreement with the Rouse model can be established. More precisely, for all q values studied (particularly for the higher ones), the $S(q,t)/S(q,0)$ curves extracted from our MD simulations through eq 16 decay more slowly than those derived on the basis of the Rouse theory through eq 17, with the spectrum of relaxation times determined through a fit to eq 10. These differences are true and not an artifact of the barostat used in the simulations to keep the pressure constant at $P = 1$ atm. In Figure 20c, for example, $S(q,t)/S(q,0)$ patterns obtained from NPT and NVT MD simulations with the same (C_{96}) *cis*-1,4-PB system at $T = 413$ K (at the same density) are compared against each other and are seen to be identical.

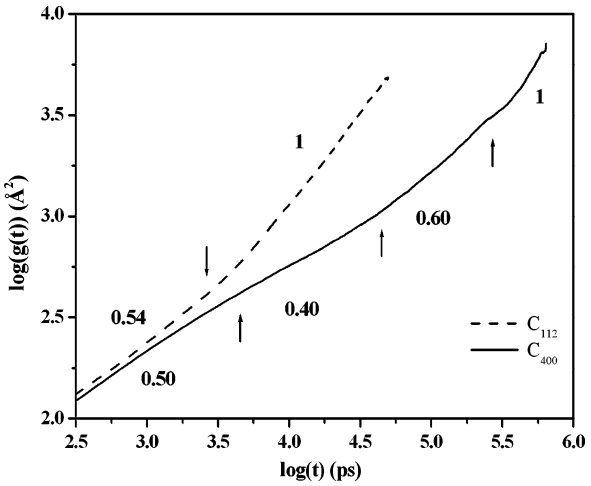

Figure 21. Mean-square displacement, $g(t)$, of the innermost chain segments against time in a log−log for the C_{112} and C_{400} *cis*-1,4-PB systems [$T = 413$ K, $P = 1$ atm].

The observation that the Rouse model cannot reproduce the dynamic structure factor of short-chain polymer melts is consistent with previous NSE measurements and MD simulations[11,13]of 1,4-PB melts and has been attributed to the non-Gaussian character of segmental displacements due to interchain correlations.[12,13] It is also important to mention that accounting for corrections in the Rouse model related to chain stiffness[16] improves only slightly the description.[39]

Mean-Square Displacement of Chain Segments, *g(t)*. Figure 21 presents results for the msd of chain segments, $g(t)$, against t calculated through

$$g(t) = \frac{1}{2n+1}\sum_{i=N/2-n}^{N/2+n}(R(i,t) - R(i,0))^2 \qquad (19)$$

in a log−log plot, with the value n denoting the number of innermost segments monitored in the course of the MD simulation (usually $n = 4-8$). Results are presented for two of the *cis*-1,4-PB systems examined here, the C_{112} and C_{400} melts at $T = 413$ K and $P = 1$ atm. The curve corresponding to the C_{112} system (dashed line) is typical of a Rouse-like behavior: for times, t, shorter than the longest relaxation or Rouse time, τ_1 (equal to about 2.5 ns for the C_{112} melt), $g(t)$ scales with time as $g(t) \approx t^{0.54}$, i.e., in agreement with what is calculated by the Rouse model for diffusion in free space for $t \ll \tau_1$, whereas for times $t \gg \tau_1$, $g(t) \approx t^1$, since the distribution of $\mathbf{R}(i,t) - \mathbf{R}(i,0)$ becomes Gaussian with variance equal to $2Dt$ (D denoting the self-diffusion constant).

In contrast to the C_{112} melt, the curve representing $g(t)$ against t for the C_{400} system (solid line) shows three

distinct breaks (marked by the arrows in Figure 21) characteristic of a system whose dynamics is governed by the reptation process. According to the reptation theory,[14] the msd of a chain segment scales with time as follows

$$g(t) \propto \begin{cases} t^{1/2} & t \le \tau_e \\ t^{1/4} & \tau_e \le t \le \tau_R \\ t^{1/2} & \tau_d \le t \le \tau_d \\ t^{1} & \tau_d \le t \end{cases} \qquad (20)$$

where τ_e denotes the onset of the effect of tube constraints (it is the time at which the segment feels the constraints imposed by the tube), τ_R the Rouse time (equal to τ_1), and τ_d the disentanglement time. The values 0.50, 0.25, 0.50, and 1 for the exponents in the four different regimes quantifying the power-law dependence of $g(t)$ on t are compared to values 0.50 ± 0.03, 0.40 ± 0.03, 0.60 ± 0.05, and 1.00 ± 0.08, respectively, obtained from our long MD simulations with the C_{400} *cis*-1,4-PB melt. The agreement of the simulation results for the four scaling laws with those proposed by the reptation theory is remarkable and provides additional evidence for the transition from a Rouse-like to a reptation-like behavior when the chain length of *cis*-1,4-PB exceeds approximately C_{200}.

V. Conclusions and Future Plans

We have presented results from very long (up to 600 ns) equilibrium atomistic MD simulations of model *cis*-1,4-PB systems, using fully equilibrated initial configurations obtained with an efficient chain-connectivity MC algorithm. A similar simulation methodology has been applied in the past to predict the terminal relaxation dynamics in linear PE.[39] All simulations were carried out with the new united-atom force field, introduced recently by Smith and Paul[9] and Smith et al.[10−13] on the basis of quantum chemistry calculations. The validity of the force field was verified through extensive comparison of our MD predictions for the structural, conformational, and thermodynamic properties of *cis*-1,4-PB to available experimental and other simulation studies, over a wide range of temperatures (ranging from $T = 298$ to 430 K) and chain lengths (ranging from C_{32} up to C_{400}).

A dramatic slowdown of the self-diffusion coefficient, D, was observed in the MD simulations when the molecular length of the *cis*-1,4-PB systems exceeded C_{200}. For systems with chain lengths $N > 200$, the power-law exponent quantifying the dependence of D on N was found to be higher than that predicted by the Rouse model and close to -2.1, in agreement with the predictions of the modified reptation theory that incorporates contour length fluctuations and constraint-release mechanisms.

By consistently mapping the atomistic trajectories onto the reptation model, we have also been able to provide estimates of the tube diameter, α, and the friction coefficient, ζ, per carbon atom. For chain lengths above C_{200}, only the reptation theory was seen to lead to chain-length independent values of ζ; in contrast, the Rouse model was unable to follow the system dynamics even qualitatively.

Additional evidence for the deviation from a Rouse-like toward a reptation-like dynamics was provided through a calculation of the relaxation times describing the terminal properties of the polymer, such as the time autocorrelation function of the end-to-end vector. Consistently with the M dependence of D and ζ, a departure from the predictions of the Rouse model toward a reptation-like behavior was observed at around C_{200}, where the longest relaxation time of chains was seen to increase rapidly with increasing M as $\tau_c \approx M^3$.

Current efforts are directed toward the simulation of significantly longer *cis*-1,4-PB systems (such as C_{500} and C_{600}), aiming at the precise definition of the critical molecular weights M_e and M_c and a more accurate estimate of the tube diameter, α.

Acknowledgment. Helpful discussions with Drs. P. Gestoso and V. Harmandaris are greatly appreciated. Financial support to G.T. provided by two Growth projects funded by DG12 of the European Commission (DEFSAM: contract no. G5RD-CT-2000-00202, and PMILS: contract no. G5RD-CT-2002-00720) are gratefully acknowledged. G.T. would also like to acknowledge the support of the European Commission through grant no. HPRI-CT-1999-00026 (the TRACS Program at EPCC).

References and Notes

(1) Mark, J. E. *J. Am. Chem. Soc.* **1966**, *88*, 4354.
(2) Abe, Y.; Flory, P. J. *Macromolecules* **1971**, *4*, 219.
(3) Li, Y.; Mattice, W. L. *Macromolecules* **1992**, *25*, 4942.
(4) Misra, S.; Mattice, W. L. *Macromolecules* **1993**, *26*, 7274.
(5) Kim, E. G.; Mattice, W. L. *J. Chem. Phys.* **1994**, *101*, 6242. Haliloğlu, T.; Bahar, I.; Erman, B.; Kim, E. G.; Mattice, W. L. *J. Chem. Phys.* **1996**, *104*, 4828.
(6) Gee, R. H.; Boyd, R. H. *J. Chem. Phys.* **1994**, *101*, 8028.
(7) Han, J.; Gee, R. H.; Boyd, R. H. *Macromolecules* **1994**, *27*, 7781.
(8) Okada, O.; Furuya, H. *Polymer*, **2002**, *43*, 971. Okada, O.; Furuya, H. *Polymer* **2002**, *43*, 977.
(9) Smith, G. D.; Paul, W. *J. Phys. Chem. A* **1998**, *102*, 1200.
(10) Smith, G. D.; Borodin, O.; Bedrov, D.; Paul, W.; Qiu, X.; Ediger, M. D. *Macromolecules* **2001**, *34*, 5192.
(11) Smith, G. D.; Paul, W.; Monkenbusch, M.; Willner, L.; Richter, D.; Qiu, X. H.; Ediger, M. D. *Macromolecules* **1999**, *32*, 8857.
(12) Smith, G. D.; Paul, W.; Monkenbusch, M.; Richter, D. *J. Chem. Phys.* **2001**, *114*, 4285.
(13) Smith, G. D.; Paul, W.; Monkenbusch, M.; Richter, D. *Chem. Phys.* **2000**, *261*, 61.
(14) Doi, M.; Edwards, S. F. *The Theory of Polymer Dynamics*; Clarendon Press: Oxford, 1986.
(15) Rouse, P. E. *J. Chem. Phys.* **1953**, *21*, 1272.
(16) Harnau, L.; Winkler, R. G.; Reineker, P. *J. Chem. Phys.* **1997**, *106*, 2469.
(17) Byutner, O.; Smith, G. D. *Macromolecules* **2001**, *34*, 134.
(18) Rochefort, W. E.; Smith, G. G.; Rachapudy, H.; Raju, V. R.; Graessley, W. W. *J. Pol. Sci., Polym. Phys. Ed.* **1979**, *17*, 1197.
(19) Carella, J. M.; Graessley, W. W.; Fetters, L. J. *Macromolecules* **1984**, *17*, 2775.
(20) Struglinski, M. J.; Graessley, W. W. *Macromolecules* **1985**, *18*, 2630.
(21) Colby, R. H.; Milliman, G. E.; Graessley, W. W. *Macromolecules* **1986**, *19*, 1261.
(22) Roovers, J. *Polym. J.* **1986**, *18*, 153. Roovers, J. *Polymer* **1985**, *26*, 1091.
(23) Colby, R. H.; Fetters, L. J.; Graessley, W. W. *Macromolecules* **1987**, *20*, 2226.
(24) Frischeknecht, A. L.; Milner, S. T. *Macromolecules* **2000**, *33*, 5273. Milner, S. T.; McLeish, T. C. B. *Phys. Rev. Lett.* **1988**, *81*, 725.
(25) English, A. D. *Macromolecules* **1985**, *18*, 178.
(26) Appel, M.; Fleischer, G.; Kärger, J.; Fujara, F.; Chang, I. *Macromolecules* **1994**, *27*, 4274.
(27) Fleischer, G.; Appel, M. *Macromolecules* **1995**, *28*, 7281.
(28) English, A. D.; Inglefield, P. T.; Jones, A. A.; Zhu, Y. *Polymer* **1998**, *39*, 309.
(29) Klein, P. G.; Adams, C. H.; Brereton, M. G.; Ries, M. E.; Nicholson, T. M.; Hutchings, L. R.; Richards, R. W. *Macromolecules* **1998**, *31*, 8871.

(30) Sen, T. Z.; Bahar, I.; Erman, B.; Lauprêtre, F.; Monnerie, L. *Macromolecules* **1999**, *32*, 3017.
(31) Graf, R.; Heuer, A.; Spiess, H. W. *Phys. Rev. Lett.* **1998**, *26*, 5738.
(32) Guillermo, A.; Cohen Addad, J. P. *J. Chem. Phys.* **2002**, *116*, 3141.
(33) Cohen Addad, J. P.; Guillermo, A. *Macromolecules* **2003**, *36*, 1609.
(34) Frick, B.; Richter, D.; Ritter, C. L. *Europhys. Lett.* **1989**, *9*, 557.
(35) Richter, D.; Frick, B.; Farago B. *Phys. Rev. Lett.* **1988**, *61*, 2465.
(36) Zorn, R.; Arbe, A.; Colmenero, J.; Frick, B.; Richter, D.; Buchenau, U. *Phys. Rev. E* **1995**, *52*, 781.
(37) Roland, C. M.; Böhm, G. G. A. *Macromolecules* **1985**, *18*, 1310.
(38) Lodge, T. P. *Phys. Rev. Lett.* **1999**, *83*, 3218. Tao, H.; Lodge, T. P.; von Meerwall, E. D.; *Macromolecules* **2000**, *33*, 1747.
(39) Harmandaris, V. A.; Mavrantzas, V. G.; Theodorou, D. N.; Kröger, M.; Ramírez, J.; Öttinger, H. C.; Vlassopoulos, D. *Macromolecules* **2003**, *36*, 1376.
(40) Kröger, M.; Ramírez, J.; Öttinger, H. C. *Polymer* **2002**, *43*, 477.
(41) Gestoso, P.; Nicol, E.; Doxastakis, M.; Theodorou, D. N. *Macromolecules* **2003**, *36*, 6925.
(42) Pant, P. V. K.; Theodorou, D. N. *Macromolecules* **1995**, *28*, 7224. Mavrantzas, V. G.; Boone, T. D.; Zervopoulou, E.; Theodorou, D. N. *Macromolecules* **1999**, *32*, 5072.
(43) Nosé, S. *Prog. Theor. Phys. Suppl.* **1991**, *103*, 1.
(44) Hoover, W. G. *Phys. Rev. A* **1986**, *31*, 1695.
(45) Tuckerman, M. E.; Berne, B. J.; Martyna, G. J. *J. Chem. Phys.* **1992**, *97*, 1990.
(46) Martyna, G. J.; Tuckerman, M. E.; Tobias, D. J.; Kein. M. L. *Mol. Phys.* **1996**, *87*, 1117.
(47) Plimpton, S. J. *J. Comput. Phys.* **1995**, *117*, 1; www.cs.sandia.gov/~sjplimp/lammps.html.
(48) Mavrantzas, V. G. Monte Carlo Simulation of Chain Molecules. In *Handbook of Materials Modeling. Volume 1: Methods and Models*; Yip, S., Ed.; Springer: The Netherlands, 2005; pp 1−15. Theodorou, D. N. Variable-connectivity Monte Carlo algorithms for the atomistic simulation of long-chain polymer systems. In *Bridging Time Scales: Molecular Simulations for the Next Decade*; Nielaba, P., Mareschal, M., Ciccotti, G., Eds.; Springer-Verlag, Berlin, 2002.
(49) Abe, M.; Fujita, H. *J. Phys. Chem.* **1965**, *69*, 3263.
(50) Moraglio, G. *Eur. Polym. J.* **1965**, *1*, 103.
(51) Hadjichristidis, N.; Zhongde, X.; Fetters, L. J.; Roovers, J. *J. Polym. Sci.: Polym. Phys.* **1982**, *20*, 743.
(52) Yi, Y. X.; Zoller, P. *J. Polym. Sci. B: Polym. Phys.* **1993**, *31*, 779.
(53) Fetters, L. J.; Lohse, D. J.; Richter, D.; Witten, T. A.; Zirkel, A. *Macromolecules* **1994**, *27*, 4639.
(54) Paul, D. R.; DiBenedetto, A. T. *J. Polym. Sci. C* **1965**, *10*, 17.
(55) Barlow, J. W. *Polym. Eng. Sci.* **1978**, *18*, 238.
(56) Pings, C. J.; Waser, J. *J. Chem. Phys.* **1968**, *48*, 3016.
(57) Frick, B.; Alba-Simionesco, C.; Andersen, K. H.; Willner, L. *Phys. Rev. E* **2003**, *67*, 051801.
(58) Ferry, J. D. *Viscoelastic Properties of Polymers*, J. Wiley and Sons: New York, 1980. Berry, G. C.; Fox, T. G. *Adv. Polym. Sci.* **1968**, *5*, 261.
(59) Doxastakis, M.; Theodorou, D. N.; Fytas, G.; Kremer, F.; Faller, R.; Müller-Plathe, F.; Hadjichristidis; N. *J. Chem. Phys.* **2003**, *119*, 6883.
(60) Bueche, F. *Physical Properties of Polymers*; Interscience: New York, 1962.
(61) Harmandaris, V. A.; Doxastakis, M.; Mavrantzas, V. G.; Theodorou, D. N. *J. Chem. Phys.* **2002**, *116*, 436.
(62) de Gennes, P. G. *J. Phys.* **1981**, *42*, 735.
(63) Kremer, K.; Binder, K. *J. Chem. Phys.* **1984**, *81*, 6381.
(64) Faller, R.; Müller-Plathe, F. *Chem. Phys. Chem.* **2001**, *3*, 180.

MA0491210